KrF Excimer Laser-induced Ozone Formation in Supercritical Carbon Dioxide

Junichiro Otomo,† Yoshito Oshima, Akinori Takami, and Seiichiro Koda*

Department of Chemical System Engineering, School of Engineering, The University of Tokyo, Hongo 7-3-1, Bunkyo-ku, Tokyo 113-8656, Japan

Received: October 5, 1999; In Final Form: January 11, 2000

Laser-induced reactions by a pulsed KrF excimer laser were studied using UV absorption spectroscopy in sub- and supercritical O_2/CO_2 mixtures up to the pressure of 15 MPa (corresponding density, 17 mol dm^{-3}). Although the 248 nm excimer laser photon energy is smaller than the energy required for dissociating O_2, ozone formation was observed in O_2/CO_2 mixtures. Under the laser irradiation, O_3 concentration increased monotonically with the increase of the irradiation time and then stayed constant, which is satisfactorily expressed by the equation $d[O_3]/dt = a - b[O_3]$. a corresponds to O_3 formation rate and b to O_3 decomposition rate constant. The value of a increased with the increase of CO_2 density up to 3 mol dm^{-3} and was then kept almost constant with further increase. O_2 absorbs a photon to yield an oxygen molecule in the Herzberg III state $O_2(A'\,^3\Delta_u)$, being augmented along with the increase of CO_2 density. In pure O_2, the predominant pathway of O_3 formation is the reaction between excited O_2 in Herzberg states and ground state O_2 to yield O_3 and atomic oxygen. In high-density O_2/CO_2 mixtures, O_3 is considered to be produced through reaction between the Herzberg states O_2 and CO_2. Taking account of the quenching effect for the above reaction together with the augmentation of O_2 absorption of laser light by the high-density CO_2, the behavior of a with respect to CO_2 density was satisfactorily explained. The behavior of b suggested a certain inhibition of O_3 recovery in high-density CO_2 after the photodecomposition of the product O_3, which was ascribed to the formation of CO_3 from the $O(^1D)$ reaction with CO_2. A certain cage effect for the O_3 photodecomposition was also suggested. No specific pressure effect was observed near the critical point.

Introduction

In our previous researches,[1,2] we carried out a photoinduced partial oxidation of hydrocarbons (ethane, cyclohexane, and ethylene) in sub- and supercritical CO_2 with irradiation of pulsed KrF excimer laser at 248 nm. Although these hydrocarbons and O_2 do not absorb KrF excimer laser light under atmospheric pressure, relatively large amounts of oxidized products were formed in the mixture of hydrocarbon/O_2/CO_2 under KrF excimer laser irradiation. Some active oxygen species should be involved. At that time, however, the mechanism of the 248 nm photoabsorption was not clear. Later we measured the absorption cross section of O_2 in pressurized CO_2 between 230 and 280 nm wavelength, and found that an absorbance of O_2 increases proportionally with the increase of the solvent CO_2 density.[3] The mechanism of the photoabsorption of O_2 was concluded to be collision-induced symmetry relaxation of the selection rule for the dipole-forbidden Herzberg III system ($A'\,^3\Delta_u \leftarrow X\,^3\Sigma_g^-$). However, subsequent reaction processes of $O_2(A'\,^3\Delta_u)$ have not been clarified.

On the other hand, supercritical CO_2 is being given attention as an alternative solvent for chemical reactions because of its unique solvent properties and nonignitability. Certain physicochemical properties, such as viscosity, diffusion constant, dielectric constant, and solubility, are related to the fluid density, which is strongly dependent on pressure and temperature, particularly near the critical point. Since the 1980s several researchers have studied chemical reactions in sub- and supercritical fluids, such as photodissociation,[4−6] recombination,[6,7] and isomerization reactions,[8,9] as well as energy transfer,[10−13] in order to clarify the solvent density effects on the reactions from a collisional energy transfer region (gaslike density) to a diffusion control region (liquidlike density).

To elucidate the laser-induced reactions of O_2 in high-density CO_2 should be useful for designing oxidation reactions in supercritical CO_2. Through a preliminary experiment, we have noticed that an appreciable amount of O_3 is produced in pressurized O_2/CO_2 mixtures under KrF excimer laser irradiation. Ozone formation is expected to occur through subsequent reaction processes of $O_2(A'\,^3\Delta_u)$. The main objective of the present research is to observe in detail O_3 formation with KrF excimer laser irradiation at 248 nm in sub- and supercritical O_2/CO_2 mixtures, and to understand the mechanism of O_3 formation. We discuss relevant elementary reactions of active oxygen species in CO_2, namely, excited oxygen molecules, O_3, oxygen atoms, CO_4, and CO_3. We also try to clarify the solvent density effect on the elementary processes.

Experimental Section

Laser irradiation experiments were carried out in a high-pressure cross-shaped optical cell made from SUS 316 of 5.0 cm^3 inner volume, which possesses four sapphire windows (diameter 1.0 cm), as shown in Figure 1. The optical length for the laser light in the cell was 3.3 cm and that for a deuterium lamp light for absorption measurement was 2.3 cm. Temperature was controlled by four Nichrome line heaters inserted into the cell block, and monitored by a thermocouple which was settled

* To whom correspondence should be addressed. Tel: +81-3-5841-7327. Fax: +81-3-5841-7255. E-mail: koda@chemsys.t.u-tokyo.ac.jp.
† E-mail: otomo@ecolab.t.u-tokyo.ac.jp.

10.1021/jp9935485 CCC: $19.00
Published on Web 03/24/2000

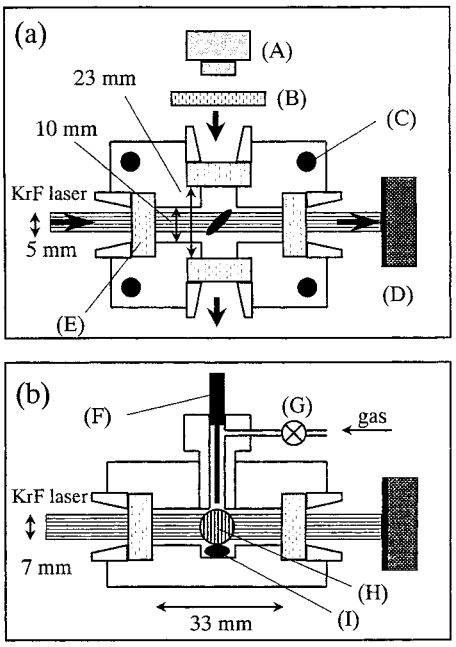

Figure 1. Illustration of reaction cell: (a) top view, (b) side view. (A) D_2 lamp, (B) $CoSO_4$ aqueous filter, (C) Nichrome line heater, (D) pyroelectric joulemeter, (E) sapphire window, (F) thermocouple, (G) stop valve, (H) the cross section of D_2 lamp light (0.79 cm^2, diameter 1.0 cm), (I) magnetic stirrer.

inside the cell at the position where direct contact with the fluid was realized. Fluid mixtures could be stirred by a magnetic stirrer.

The experimental procedures were as follows. The optical cell was evacuated prior to the sample preparation. Then O_2 was introduced into the cell up to a given pressure (typical O_2 pressure, 1.97 MPa), which was followed by the introduction of CO_2 up to a desired pressure using a HPLC pump (JASCO Co., PU-980). Pressure was detected by a pressure transmitter (KOFLOC, KH15). The cell was maintained at 308 ± 0.1 K. The contents were stirred by a magnetic stirrer for 5 min before irradiation. Carbon dioxide (Suzuki Shokan Co. Ltd.; purity >99.7%) and O_2 (Suzuki Shokan Co. Ltd.; purity >99.7%) were used as received.

Unfocused light pulses at 248 nm from a KrF excimer laser (Lambda physics, EMG53MSS-1) were introduced along the 3.3 cm path of the optical cell. The typical pulse energy at the entrance window was 3.8 mJ $pulse^{-1}$, and the repetition rate 10 Hz. The laser beam cross section, which had an elliptical shape (major axis ≈ 7 mm, minor axis ≈ 5 mm), was about 0.27 cm^2 as drawn in Figure 1. The laser intensity was monitored with a pyroelectric joulemeter (Gentec, ED-500).

During the KrF excimer laser irradiation, absorbance of O_3 was measured at 255 nm through the 2.3 cm path perpendicular to the irradiated laser beam. A deuterium lamp (Hamamatsu Photonics, L1626) was used as the light source. The deuterium lamp light was first passed through a cell of 1 cm thickness containing $CoSO_4$ aqueous solution (0.05 mol dm^{-3}) to cut the light shorter than 210 nm. The cross section of the deuterium lamp light had a circular shape of diameter 10 mm as drawn in Figure 1. Absorption spectra were dispersed by a 75 cm monochromator (Jobin-Yvon, HRS2) and detected by a photomultiplier (Hamamatsu Photonics, R928; detection range, 185−900 nm). The output signal was amplified and recorded on a personal computer. During the laser irradiation, the contents of the cell were stirred by the magnetic stirrer.

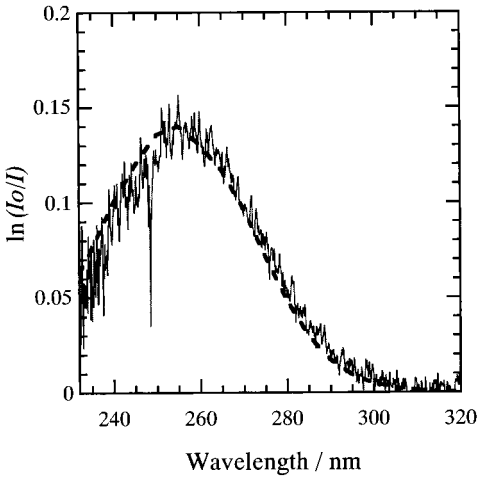

Figure 2. Absorption spectrum ($B(1^1B_2) \leftarrow X(1^1A_1)$) of ozone. Solid line: experimental profile. Dotted line: spectrum of the absorption cross section of ozone, $B(1^1B_2) \leftarrow X(1^1A_1)$ transition, which is scaled at the experimental peak position. Experimental conditions: O_2 2.94 MPa (1.18 mol dm^{-3}), total density 12.0 mol dm^{-3}, CO_2 balance, temperature 308 K, pulse energy 3.8 mJ $pulse^{-1}$, laser repetition rate 10 Hz.

We checked the influence of the deuterium lamp light on O_3 formation and found no detectable influence. We also investigated the spatial distribution of O_3 concentration in the cell, changing the diameter of the spot of deuterium lamp light at the total pressure of 10.1 MPa. Using a 5 mm and a 10 mm diameter of the cross section of the deuterium lamp light, the observed O_3 concentrations were the same, which indicated that the O_3 concentration distribution was almost homogeneous in the cell due to the stirring.

The densities of O_2/CO_2 mixture in gas and supercritical phases were estimated by the Peng−Robinson equation[14] adopting appropriate parameters (CO_2: critical temperature (T_c) 304.2 K, critical pressure (P_c) 7.38 MPa, critical density (ρ_c) 10.6 mol dm^{-3}; and O_2: T_c 154.6 K, P_c 5.05 MPa, ρ_c 13.6 mol dm^{-3}). As the binary interaction parameter, k_{ij}, for O_2-CO_2, we employed that for N_2-CO_2 ($k_{ij} = -0.017$),[15] because the former value is not reported. We investigated pressure effects in O_2/CO_2 mixtures, keeping the amount of O_2 in the cell constant. Thus, the mole fraction of individual components and also the critical point of the mixture change continuously with the increase of CO_2 pressure. The estimation method of the critical point of fluid mixtures was presented by Liu.[16] In the typical mixture with 1.97 MPa O_2 at 308 K (the corresponding O_2 density, 0.78 mol dm^{-3}), the experimental temperature (308 K) is higher than the critical temperature of the mixture at any total pressure. The region where the total pressure is smaller than 8.0 MPa (the corresponding total density is 5.2 mol dm^{-3}) is estimated to be in the gas phase because the total pressure is smaller than the critical pressure of the mixture. When the total pressure is larger than 8.0 MPa, the region is regarded to be in supercritical phase.

Results

Products. A broad absorption between 230 and 300 nm represented by a solid line in Figure 2 was generated in O_2/CO_2 mixtures with KrF excimer laser irradiation. The spectrum in Figure 2 was already corrected for the contribution of O_2 absorption. The noise at about 250 nm is due to the scattered KrF excimer laser light at 248 nm. The dotted line shows the absorption spectrum of Hartley band ($B(1^1B_2) \leftarrow X(1^1A_1)$) of O_3 which is scaled to the experimental value at the experimental

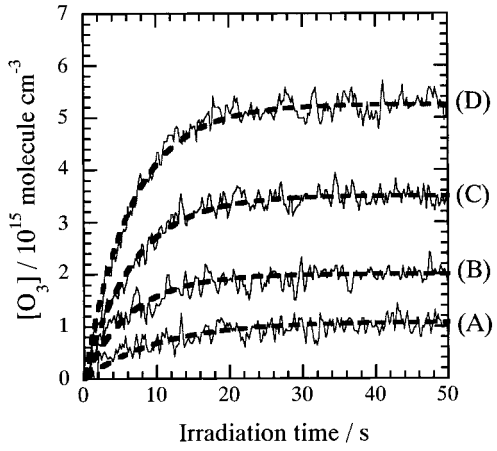

Figure 3. Typical time profiles of ozone concentration with KrF excimer laser irradiation. Solid line: observed profile. Dotted line: simulation from eq 2. Experimental conditions: total density 11.9 mol dm^{-3}, CO_2 balance, temperature 308 K, pulse energy 3.8 mJ $pulse^{-1}$, laser repetition rate 10 Hz. (A) O_2 0.49 MPa (0.19 mol dm^{-3}), $a = 1.1 \times 10^{14}$ molecule cm^{-3} s^{-1}, $b = 0.10$. (B) O_2 0.98 MPa (0.39 mol dm^{-3}), $a = 3.1 \times 10^{14}$ molecule cm^{-3} s^{-1}, $b = 0.15$. (C) O_2 1.97 MPa (0.78 mol dm^{-3}), $a = 5.2 \times 10^{14}$ molecule cm^{-3} s^{-1}, $b = 0.15$. (D) O_2 2.94 MPa (1.17 mol dm^{-3}), $a = 8.0 \times 10^{14}$ molecule cm^{-3} s^{-1}, $b = 0.15$.

peak maximum. Both profiles accord with each other, showing that O_3 is generated in O_2/CO_2 mixtures with KrF excimer laser irradiation. No other appreciable absorption was detected in the UV and visible regions.

Ozone concentration was calculated from the absorbance of O_3 at 255 nm, adopting the absorption cross section in the gas phase at 255 nm (1.16×10^{-17} cm^2 $molecule^{-1}$).[17] Because the Hartley band ($B(1^1B_2) \leftarrow X(1^1A_1)$) of O_3 is an allowed transition, the O_3 absorption cross section is expected to be almost independent of the solvent density. We have indeed found experimentally that the relative value of the O_3 absorption cross section is kept constant within ±10% in the total density between 1 and 12 mol dm^{-3}. Troe and co-worker calculated the O_3 concentration in dense N_2, Ar, and He media without taking account of any pressure dependence of the O_3 cross section.[7] They employed an O_3 absorption cross section of 9×10^{-18} cm^2 $molecule^{-1}$ at 265 nm that accords with the present value at 255 nm, taking wavelength dependence of the absorption cross section into account.

Time Profile of Ozone Formation. Typical time profiles of O_3 concentration plotted against the irradiation time are presented by solid lines in Figure 3. The O_3 concentration increased monotonically with the irradiation time, and then it reached a constant value. Here, it should be noted that the concentration corresponds to the accumulated O_3 concentration from individual laser pulses during the irradiation time.

We tried to analyze the time dependence of O_3 concentration by the following equation containing two terms: O_3 formation rate, a, and O_3 decomposition rate, $b[O_3]$:

$$d[O_3]/dt = a - b[O_3] \quad (1)$$

Integrating it, we obtain

$$[O_3] = (a/b)(1 - e^{-bt}) \quad (2)$$

Experimental time profiles of O_3 concentration were fitted to eq 2 by the least-squares method for nonlinear equations (Levenberg−Marquardt method),[18] using a and b values as fitting parameters. The calculated time profiles, adopting the determined a and b values, are presented by dotted lines in Figure 3 that satisfactorily accord with the experimental data. Equation 2, thus, can explain the time profiles of the O_3 concentration adequately. In the following sections, we will show the determined a and b values as the functions of pulse energy, O_2 concentration and solvent density.

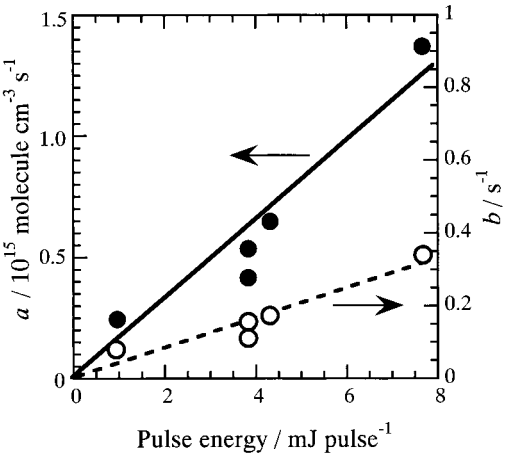

Figure 4. Pulse energy dependence of ozone formation rate, a, and ozone decomposition rate constant, b. Filled circles: ozone formation rate, a. Open circles: ozone decomposition rate constant, b. Experimental conditions: O_2 1.97 MPa (0.78 mol dm^{-3}), total density 11.8 mol dm^{-3}, CO_2 balance, temperature 308 K, laser repetition rate 10 Hz.

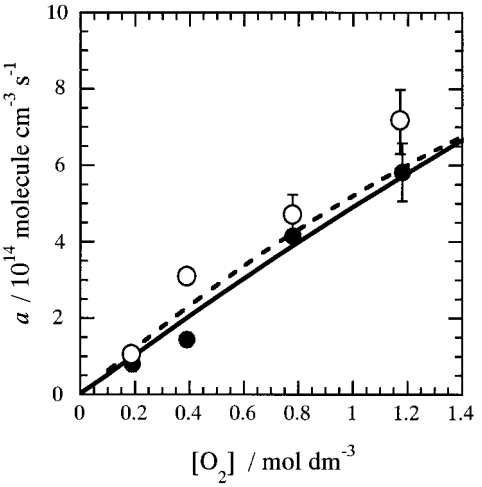

Figure 5. Ozone formation rate, a, as a function of the O_2 concentration at constant total densities. Filled circles: observed values at 5.0 mol dm^{-3} of the total density. Open circles: observed values at 12.0 mol dm^{-3} of the total density. Solid line: prediction from eq 18 at 5.0 mol dm^{-3} of the total density ($k_{17}/k_{16} = 0.9 \times 10^{-21}$ cm^3 $molecule^{-1}$). Dotted line: prediction from eq 18 at 12.0 mol dm^{-3} of the total density ($k_{17}/k_{16} = 0.9 \times 10^{-21}$ cm^3 $molecule^{-1}$). Experimental conditions: temperature 308 K, CO_2 balance, pulse energy 3.8 mJ $pulse^{-1}$, laser repetition rate 10 Hz.

Ozone Formation Rate (a). The O_3 formation rate (a) under a supercritical condition (total density, 11.8 mol dm^{-3}) shows a linear dependence on the pulse energy as shown in Figure 4.

The a values are plotted against O_2 concentration in gas phase (total density, 5.0 mol dm^{-3}) and in supercritical phase (total density, 12.0 mol dm^{-3}) in Figure 5. The inserted curves are estimated according to the reaction model as will be described later. The present results show that a is almost proportional to the first order of O_2 concentration, independent of the CO_2 density.

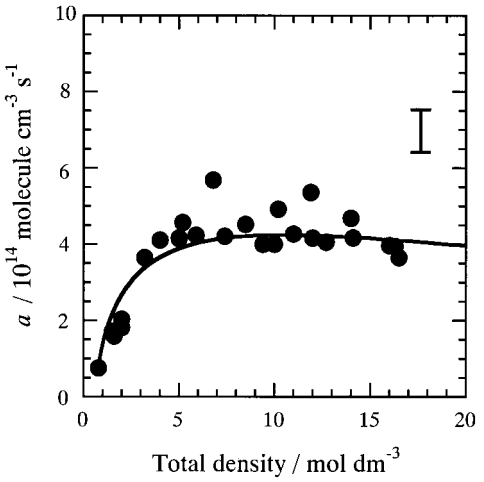

Figure 6. Ozone formation rate, *a*, as a function of the total density. Filled circles: observed values. Solid line: prediction from eq 18 ($k_{17}/k_{16} = 0.9 \times 10^{-21}$ cm^3 molecule^{-1}). Experimental conditions: O_2 1.97 MPa (0.78 mol dm^{-3}), CO_2 balance, temperature 308 K, pulse energy 3.8 mJ pulse^{-1}, laser repetition rate 10 Hz. The range of the data scattering is shown by the error bar in the figure.

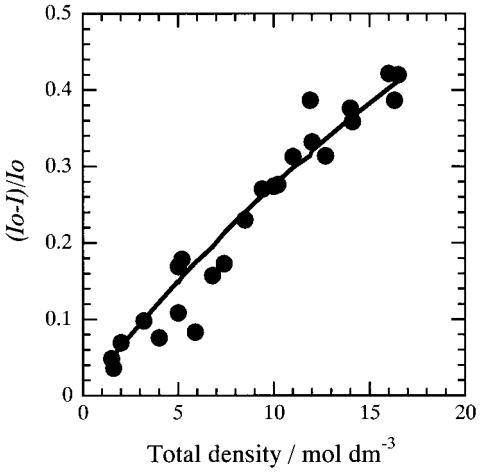

Figure 7. Fraction of the 248 nm light extinction, $(I_0 - I)/I_0$, plotted against the total density. Filled circles: experimental fraction from which the contribution of ozone is already subtracted. Solid line fraction of the absorbance of O_2 predicted from eq 3. Experimental conditions: O_2 1.97 MPa (0.78 mol dm^{-3}), CO_2 balance, temperature 308 K, pulse energy 3.8 mJ pulse^{-1}, laser repetition rate 10 Hz.

The dependence of *a* on the total density at a constant O_2 partial pressure is shown by filled circles in Figure 6. The inserted curve is also estimated from the reaction model described later. As the CO_2 density increases, the value of *a* increases monotonically in the region of the total density smaller than 3 mol dm^{-3}, and then remains constant in the region of the total density larger than 3 mol dm^{-3}.

Absorption of KrF Excimer Laser Light by O_2. We measured the extinction of the irradiation laser light at 248 nm as a function of the total density, when the O_3 concentration reached a constant value. In Figure 7, the fraction, $(I_0 - I)/I_0$, from which the contribution of O_3 absorption is already subtracted, is plotted against the total density. It increases with the increase of the CO_2 density.

The photoabsorption augmentation of O_2 Herzberg bands and Herzberg continuum by O_2 itself and by some foreign gases (N_2, CO_2) has been extensively studied in gas and supercritical phases.[3,19−23] It is concluded that the photoabsorption augmentation of the Herzberg III system ($A'\,^3\Delta_u \leftarrow X\,^3\Sigma_g^-$) corresponding

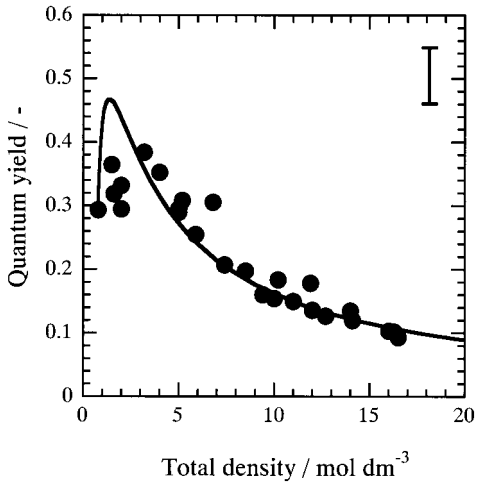

Figure 8. Quantum yield of ozone formation, ϕ, as a function of the total density. Filled circles: experimental values. Solid line prediction from eq 20 ($k_{17}/k_{16} = 0.9 \times 10^{-21}$ cm^3 molecule^{-1}). Experimental conditions: O_2 1.97 MPa (0.78 mol dm^{-3}), CO_2 balance, temperature 308 K, pulse energy 3.8 mJ pulse^{-1}, laser repetition rate 10 Hz. The range of the data scattering is shown by the error bar in the figure.

to a transition with $\Delta\Lambda = 2$ is induced by the collision-induced relaxation of the angular momentum selection rule, due to the perturbation by O_2 and/or by foreign gases.[3,23] The Herzberg III absorption in O_2/CO_2 mixtures has the density-sensitive cross section expressed by the following equation:

$$\sigma_{\text{total}} = \sigma_0 + \sigma_{1(O_2)}\rho_{(O_2)} + \sigma_{1(CO_2)}\rho_{(CO_2)} \qquad (3)$$

where σ_{total} is the total cross section, σ_0 is the cross section at zero pressure, $\sigma_{1(i)}$ is the density coefficient of component *i*, and $\rho_{(i)}$ is the density of component *i*.[3] The estimated fraction of 248 nm light extinction from eq 3 is shown as a solid line in Figure 7 for the typical experiments with 0.78 mol dm^{-3} O_2, employing the values of σ_0 and $\sigma_{1(i)}$ from the previous research: $\sigma_0 = 3 \times 10^{-25}$ cm^2 molecule^{-1}, $\sigma_{1(O_2)} = 3.71 \times 10^{-44}$, and $\sigma_{1(CO_2)} = 3.45 \times 10^{-44}$ cm^5 molecule^{-1} at 248 nm.[3] The estimated fraction has a good agreement with the experimental fraction.

Thus, we estimated the quantum yield of O_3 formation corresponding to the *a* value on the basis of the O_2 absorption which was estimated from eq 3. Figure 8 shows the quantum yield (filled circles), which increases in the low total density region and then decreases with the increase of the total density. The curve in the figure is estimated from the reaction model described later.

Ozone Decomposition Rate Constant (*b*). The values of *b* are already plotted against the laser pulse energy in Figure 4, which increases proportionally with the increase of laser pulse energy. On the other hand, the dependence of *b* on the O_2 concentration at two constant total densities (5.0 and 12.0 mol dm^{-3}) in Figure 9 shows that the value stays constant with respect to the O_2 concentration. The dependence of *b* on CO_2 density is shown by the filled circles in Figure 10a. With the increase of CO_2 density, the value increases in the region of the total density smaller than 3 mol dm^{-3}, reaches a peak at around 5 mol dm^{-3} of the total density, and then slightly decreases with respect to the CO_2 density.

Discussion

Ozone Formation Process in Pressurized O_2. Several researchers studied O_3 formation with KrF excimer laser

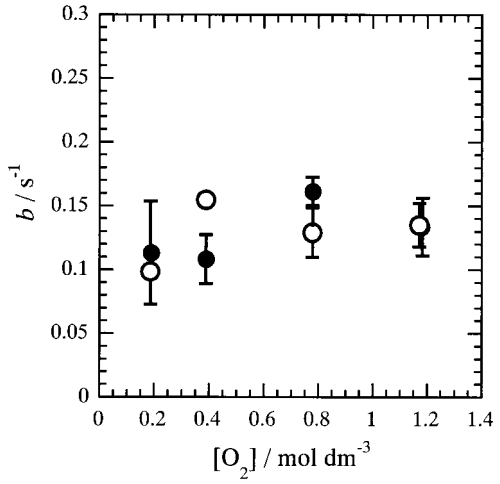

Figure 9. Ozone decomposition rate constant, *b*, as a function of the O_2 concentration at constant total densities. Filled circles: values at 5.0 mol dm^{-3} of the total density. Open circles: values at 12.0 mol dm^{-3} of the total density. Experimental conditions: temperature 308 K, CO_2 balance, pulse energy 3.8 mJ $pulse^{-1}$, laser repetition rate 10 Hz.

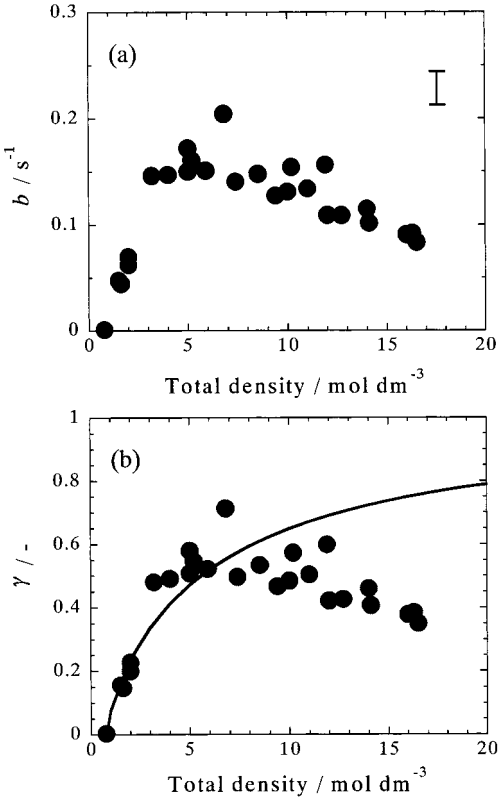

Figure 10. Ozone decomposition rate constant, *b*, and γ value as a function of the total density. (a) Filled circles: observed *b* values. The range of the data scattering is shown by the error bar. (b) Filled circles: observed γ values. Solid line: prediction from eq 30 ($k_{27}/k_{28} = 3 \times 10^{21}$ molecule cm^{-3}). Experimental conditions: temperature 308 K, CO_2 balance, pulse energy 3.8 mJ $pulse^{-1}$, laser repetition rate 10 Hz.

irradiation from O_2 in gas phase. It is important to note that the energy of 248 nm light is smaller by 0.12 eV (11.1 kJ mol^{-1}) than the dissociation threshold of O_2 at 242.4 nm.[24] Slanger et al.[25] first found that O_3 is produced from unfocused KrF excimer laser irradiation to pure O_2. Afterwards, Shi and Barker[26] studied the reaction between electronically excited O_2 in the Herzberg states ($A\ ^3\Sigma_u^+$, $A'\ ^3\Delta_u$, $c\ ^1\Sigma_u^-$) and ground state $O_2(X)$, and claimed that O_3 and atomic oxygen are formed through the above reaction. Brown and Vaida[27] who studied the photochemistry of $(O_2)_2$ dimers in cold jet with resonance-enhanced multiphoton ionization claimed that $A'\ ^3\Delta_u + X\ ^3\Sigma_g^- \leftarrow X\ ^3\Sigma_g^- + X\ ^3\Sigma_g^-$ transition of $(O_2)_2$ dimer takes place from 251 to 266 nm, which subsequently yields O_3 and atomic oxygen to some extent.

As already mentioned, $O_2(A'\ ^3\Delta_u)$ is generated through O_2 absorption at 248 nm. The fact that $O_2(A'\ ^3\Delta_u)$ is almost isoenergetic with $O_2(A\ ^3\Sigma_u^+)$ and $O_2(c\ ^1\Sigma_u^-)$ might cause a rapid internal conversion and/or intersystem crossing among the Herzberg states ($A\ ^3\Sigma_u^+$, $A'\ ^3\Delta_u$, and/or $c\ ^1\Sigma_u^-$). The excited $O_2(A\ ^3\Sigma_u^+, A'\ ^3\Delta_u, c\ ^1\Sigma_u^-)$ is considered to react with the ground state $O_2(X\ ^3\Sigma_g^-)$ according to Shi and Barker,[26] although we cannot identify which Herzberg state eventually reacts with $O_2(X)$. Thus, the reaction mechanism of O_3 formation in gas phase O_2 is represented as follows.

$$O_2(X) + 248\ \text{nm} \rightarrow O_2(A') \tag{4}$$

$$O_2(A') \rightleftarrows O_2(A,c) \tag{5}$$

$$O_2(A,A',c) + O_2(X) \rightarrow O_3 + O(^3P) \tag{6a}$$

$$\rightarrow O_2(X) + O_2(X) \tag{6b}$$

Under the present experimental conditions, $O(^3P)$ generated through reaction 6a exclusively reacts with O_2 to yield O_3:

$$O(^3P) + O_2(X) + M \rightarrow O_3 + M \tag{7}$$

Since the O_2 absorbance at 248 nm is smaller than 3% in the present experiments, O_2 absorption is approximately represented by $\sigma_{1(O_2)}[O_2]^2L$ from eq 3, where *L* is the optical length (3.3 cm) along the laser axis. The contribution of σ_0 can be neglected under the present experimental condition of high-pressure O_2. Thus, the O_3 formation rate (*a*) is expressed as

$$a = \frac{2I\eta\sigma_{1(O_2)}[O_2]^2L}{V} \tag{8}$$

Here, η is the branching fraction of reaction 6a, *V* is the cell volume, and *I* is the laser intensity (photon s^{-1}) which is estimated at the center of the cell. The linear energy dependence of eq 8 is consistent with the result in Figure 4. We estimated the η value by dividing the observed *a* value by $2I\sigma_{1(O_2)}[O_2]^2L/V$ according to eq 8, and obtained $\eta = 0.15 \pm 0.01$ in pure O_2 from 0.98 to 1.97 MPa. Similarly, we estimated the η value from the experimental data of Shi and Barker,[26] and obtained $\eta = 0.12-0.15$ in pure O_2 from 0.03 to 0.21 MPa. It is important to note that the values from the present work and Shi and Barker's experiments are very close, which guarantees that the principal O_3 formation mechanism is the same in pure O_2.

Slanger and Shi also discussed an autocatalytic mechanism of the O_3 formation[25,26] via vibrationally excited $O_2^\dagger$ ($X\ ^3\Sigma_g^-$) produced through subsequent photolysis of the product O_3 within the same laser pulse.

$$O_3 + 248\ \text{nm} \rightarrow O(^1D) + O_2(a\ ^1\Delta_g) \tag{9}$$

$$\rightarrow O(^3P) + O_2^\dagger(X\ ^3\Sigma_g^-) \tag{10}$$

$$O_2^\dagger(X) + 248\ \text{nm} \rightarrow O_2(B\ ^3\Sigma_u^-) \rightarrow 2O(^3P) \tag{11}$$

$$O_2^{\dagger}(X) + M \rightarrow O_2(X) + M \quad (12)$$

$$O(^3P) + O_2(X) + M \rightarrow O_3 + M \quad (7)$$

We estimated the contribution of the above autocatalytic mechanism for the O_3 formation rate (a) under the present experimental conditions as discussed below. First, the amount of $O_2^{\dagger}(X)$ obtained from reaction 10 was estimated, using the absorption cross section of O_3 at 248 nm (1.07×10^{-17} cm^2 molecule^{-1}),[17] the branching fraction of reaction 10 ($\phi \approx 0.1$),[25,28] and the employed laser power. Second, the amount of regenerated O_3 through reactions 11, 12, and 7 was estimated. As the absorption cross section for reaction 11, we employed the empirical value, 1.5×10^{-18} cm^2 molecule^{-1}, from the literature.[26] The quenching rate constants by O_2 or CO_2 for reaction 12 are reported to be $10^{-13}-10^{-15}$ cm^3 molecule^{-1} s^{-1}.[29−31] Finally, we found the contribution of the autocatalytic mechanism for a is smaller than 10% in pure O_2 at the present typical condition (density 0.78 mol/dm^3). It becomes smaller than 1% when the total density is larger than 5 mol/dm^3 in O_2/CO_2 mixtures.

In addition, while highly vibrationally excited $O_2^{\dagger}(X)$ from reaction 10 was expected to react with ground state $O_2(X)$ to yield O_3 and atomic oxygen,[32] recent ab initio calculation has denied any important contribution of the above reaction.[33] In conclusion, the autocatalytic reaction through the production of vibrationally excited $O_2^{\dagger}(X)$ is not important under the present experimental conditions.

Ozone Formation Process in O_2/CO_2 Mixtures. In O_2/CO_2 mixtures, O_2 photoabsorption is augmented by CO_2 as well as by O_2 itself. It is important to investigate whether CO_2 also plays the role of producing O_3 or not. At first, we will assume that CO_2 only acts as a collisional quencher of excited O_2 in Herzberg states. The relevant processes are

$$O_2(X) + 248\ \text{nm} \rightarrow O_2(A') \quad (4)$$

$$O_2(A') \rightleftarrows O_2(A,c) \quad (5)$$

$$O_2(A,A',c) + CO_2 \rightarrow O_2(X) + CO_2 \quad (13)$$

$$O_2(A,A',c) + O_2(X) \rightarrow O_3 + O(^3P) \quad (6a)$$

$$\rightarrow O_2(X) + O_2(X) \quad (6b)$$

Thus, the O_3 formation rate (a) is expressed as

$$a = \frac{2IL}{V}(\eta\sigma_{1(O_2)}[O_2]^2 + \eta\sigma_{1(CO_2)}[CO_2] \times [O_2])\frac{k_6[O_2]}{k_6[O_2] + k_{13}[CO_2]} \quad (14)$$

The meanings of V, L, I, η, and σ_1 in eq 14 are the same as those in eq 8.

We tried to estimate the value of a by eq 14. Because the collisional removal rate constant of $O_2(A')$ has not been reported,[34−37] we employed the collisional removal rate constants of $O_2(A,v=7)$ as k_6 and k_{13},[36] considering that the energy difference between $O_2(A,v=7)$ and $O_2(X,v=0)$ is nearly equal to the 248 nm photon energy. Equation 14 then predicts that most excited $O_2(A,A',c)$ molecules are electronically quenched by CO_2, because $k_{13}[CO_2]$ is much larger than $k_6[O_2]$ under the present conditions. The predicted O_3 yield is, therefore, only 10% of the experimental value under the typical total density of 10 mol dm^{-3}. Also eq 14 cannot reproduce the first order O_2 concentration dependence of a shown in Figure 5, because eq 14 implies almost the second order of O_2 concentration dependence of a. According to the above discussion, it is suggested that some additional mechanism is present to produce atomic oxygen or O_3 from $O_2(A,A',c)$.

We will consider the possibility of O_3 formation via CO_4 intermediate species from excited O_2 and CO_2. Recently, CO_4 molecule was studied by ab initio method by several researchers.[38−40] The following processes on singlet and triplet potential energy surfaces are plausible.

$$O_2(c\ ^1\Sigma_u^-) + CO_2(X\ ^1\Sigma_g^+) \rightarrow CO_4(1^1A_1) \quad (15a)$$

$$O_2(A\ ^3\Sigma_u^+, A'\ ^3\Delta_u) + CO_2(X\ ^1\Sigma_g^+) \rightarrow CO_4(1^3B_1) \quad (15b)$$

$$CO_4(1^1A_1) \rightarrow O_3(X\ ^1A_1) + CO(X\ ^1\Sigma_g^+) \quad (16a)$$

$$CO_4\ (1^3B_1) \rightarrow CO_3(X\ ^1A_1) + O(^3P) \quad (16b)$$

According to Averyanov's calculation,[38,39] reaction 15a is energetically possible under the 248 nm irradiation (exothermic by 0.56 eV), while the required energy for reaction 15b is larger by 0.56 eV than the energy of 248 nm light. However, taking the uncertainties in ab initio calculations into account, both singlet and triplet reaction paths cannot be denied at present. Indeed, the energy level of $CO_4(1^1A_1)$ by ab initio second-order Møller−Plesset (MP2) level from several researchers[38,40] scatters in the range of 0.4 eV.

Reactions 16a and 16b are considered to be exothermic reactions, although the energy level of $CO_3(X\ ^1A_1, C_{2v})$ by MP2 level[38,41−43] scatters in the range of 2.5 eV. The produced $O(^3P)$ from reaction 16b exclusively converts to O_3 under the present condition, and thus the discrimination between reaction 16a and 16b is impossible so long as only O_3 formation is concerned. In order to check the possibility of CO formation, we tried to detect CO production in O_2/CO_2 mixture gas-chromatographically (Shimadzu, GC-8APT; column, Unibeads C) after the KrF excimer laser irradiation. We, however, failed to observe CO formation, which indicates that the relative contribution of reaction 16a to 16b should be lower than 2%, considering the detection limit of CO by the employed gas-chromatographic measurement. The plausible reaction, thus, proceeds through reactions 15b and 16b.

Taking the decrease of the quantum yield of O_3 formation with the increase of solvent CO_2 density into consideration, the quenching process of CO_4 may occur in parallel with reaction 16, as presented by reaction 17.

$$CO_4 + M \rightarrow CO_2 + O_2 + M \quad (17)$$

From the above discussion, the O_3 formation rate (a) is expressed as

$$a = \frac{ILY}{V} \quad (18)$$

where

$$Y = 2\eta(\sigma_{1(O_2)}[O_2]^2 + \sigma_{1(CO_2)}[CO_2][O_2])\frac{k_6[O_2]}{k_6[O_2] + k_{15}[CO_2]} + (\sigma_{1(O_2)}[O_2]^2 + \sigma_{1(CO_2)}[CO_2] \times [O_2])\frac{k_{15}[CO_2]}{k_6[O_2] + k_{15}[CO_2]}\frac{k_{16}}{k_{17}[M] + k_{16}} \quad (19)$$

Here, we will predict the a value by eq 18. We employ the collisional removal rate constants of $O_2(A,v=7)$ as k_6 and k_{15} ($k_6 = 3.5 \times 10^{-11}$ cm^3 molecule^{-1} s^{-1}, $k_{15} = 7.2 \times 10^{-11}$ cm^3 molecule^{-1} s^{-1})[36] as previously. Figure 6 shows that a successful agreement between the experimental data and the prediction from eq 18 is obtained when we employ 0.9×10^{-21} cm^3 molecule^{-1} as the value of k_{17}/k_{16}. As shown in Figure 5, the O_2 concentration dependence of a is also explained well by eq 18. When k_{17} is assumed to be 10^{-11} cm^3 molecule^{-1} s^{-1}, k_{16} should be on the order of 10^{10} s^{-1}, which is within a plausible range as a unimolecular decomposition rate constant.[44] However, further quantitative analysis for the validity of the k_{17}/k_{16} value may be needed.

The quantum yield of O_3 formation is then expressed by

$$\phi = Y/(\sigma_{1(O_2)}[O_2]^2 + \sigma_{1(CO_2)}[CO_2][O_2]) \quad (20)$$

The prediction from eq 20 shows a good agreement with the experimental data as shown in Figure 8. In conclusion, reaction between excited O_2 and CO_2 should be responsible for the formation of O_3 in high-density O_2/CO_2 mixtures, although CO_2 is generally considered as an inactive solvent.

Ozone Photolysis and Subsequent Processes. As already mentioned, when O_3 is photodissociated in the Hartley band under the 248 nm irradiation, a singlet channel and a triplet channel are obeyed as shown by the following equations.

$$O_3 + 248\ \text{nm} \rightarrow O(^1D) + O_2\ (a\ ^1\Delta_u) \quad (9)$$

$$\rightarrow O(^3P) + O_2^{\dagger}(X\ ^3\Sigma_g^-) \quad (10)$$

The quantum yield is reported to be 0.85−0.9 into the singlet channel, and 0.15−0.1 into the triplet channel at 248 nm.[25,28] Because the O_3 absorbance at 248 nm is smaller than 20% in the present experiments, O_3 absorption can be approximately represented by $\sigma[O_3]L$. Therefore, the rate of the O_3 photodissociation is expressed by the following equation:

$$\frac{d[O_3]}{dt} = -\frac{\phi I\sigma L}{V}[O_3] \quad (21)$$

where ϕ is the total quantum yield of eqs 9 and 10, which is equal to 1, V is the cell volume, σ is the absorption cross section of O_3 at 248 nm, and L is the optical length. I is the laser intensity expressed by photon number per second and is estimated at the center of the cell.

There is some possibility that O_3 is regenerated through subsequent processes. Thus, the O_3 decomposition rate, $b[O_3]$, in eq 1 should be expressed by the following equation.

$$b[O_3] = \gamma\frac{\phi I\sigma L}{V}[O_3] \quad (22)$$

Here, γ empirically represents the efficiency of the decomposition of O_3, which is defined as (photodissociated O_3 − regenerated O_3)/photodissociated O_3. Equation 22 implies $b \propto I$, and the result of the pulse energy dependence in Figure 4 is consistent with this proposed relationship. Provided that γ is not dependent on O_2 concentration, b is also independent of it. Indeed, it is found in Figure 9 that b is kept constant with respect to O_2 concentration. Concerning the dependence of γ on the total density, experimentally determined γ values from Figure 10a and eq 22 are plotted in Figure 10b. Under the typical condition ($\phi = 1$, $I \approx 4.0 \times 10^{16}$ photon s^{-1}, $V = 5.0$ cm^3, $\sigma = 1.07 \times 10^{-17}$ cm^2 molecule^{-1}, $L = 3.3$ cm), $\phi I\sigma L/V$ is calculated to be 0.28.

We will consider the dependence of γ value on the total density based on a possible reaction mechanism. In gas phase, it is reported that $O(^1D)$ generated by photodissociation of O_3 is deactivated through collision with CO_2.[45]

$$O(^1D) + CO_2 \rightarrow O(^3P) + CO_2 \quad (23)$$

Subsequent reactions of $O(^3P)$ are considered to regenerate O_3.

$$O(^3P) + O_2(X) + M \rightarrow O_3 + M \quad (7)$$

When reaction 23 proceeds exclusively, the value of γ is expected to be 0, because the same amount of O_3 regenerates through reaction 7. In the present experiments where pure O_2 (the total density is the same as $[O_2]$ of 0.78 mol dm^{-3}) is irradiated, the experimental b and γ values are actually very small ($b = 0.0009$, $\gamma = 0.003$) as shown in Figure 10a,b. The value of b, however, has been found to increase with the increase of CO_2 density. In the region where the total density is larger than 3 mol dm^{-3}, b has the value of around 0.15. The corresponding value of γ is approximately 0.5 as shown in Figure 10b, which indicates that there should be another reaction mechanism in which $O(^1D)$ or $O(^3P)$ is trapped so as to suppress the regeneration of O_3.

Froese et al.[41] calculated the reaction pathway on a singlet energy surface of $O(^1D) + CO_2(^1\Sigma_g^+)$ and a triplet energy surface of $O(^3P) + CO_2(^1\Sigma_g^+)$ by ab initio method. They claimed that the intersystem crossing from the singlet surface to the triplet surface may occur through the formation of CO_3 and that the reaction pathway on the singlet surface leads to a bound region of the singlet surface where CO_3 intermediates of C_{2v} and D_{3h} geometry exist. Their energies are lower by 163 kJ mol^{-1} (C_{2v}) and by 146 kJ mol^{-1} (D_{3h}) than $O(^1D) + CO_2(^1\Sigma_g^+)$, respectively.

Experimental evidence for the existence of CO_3 in condensed CO_2 was given in previous researches. Several researchers[46−48] observed the formation of CO_3 in CO_2 matrix through the reaction of CO_2 and $O(^1D)$. DeMore et al.[49] investigated the 253.7 nm photolysis of O_3 in liquid CO_2 (228 K, density: 25.8 mol/dm^3). They discussed that the quantum yield of O_3 disappearance is controlled by the following reactions.

$$O(^1D) + CO_2 + M \rightarrow CO_3 + M \quad (24)$$

$$CO_3 + CO_3 \rightarrow 2CO_2 + O_2 \quad (25)$$

In the present experiments, a similar mechanism should be obeyed. However, reaction 25 may not be an elementary reaction, and the initial process may proceed as follows:

$$CO_3(X\ ^1A_1) + CO_3(X\ ^1A_1) \rightarrow CO_4(1^1A_1) + CO_2(X\ ^1\Sigma_g^+) \quad (25a)$$

because the above spin-allowed reaction 25a is exothermic according to Averyanov's ab initio calculation.[38] Most of produced $CO_4(1^1A_1)$ are likely to decompose into CO_2 and O_2

through eq 17 as discussed later, and thus O_3 is not expected to be regenerated to a meaningful amount through the CO_3 reactions. It is, thus, plausible that the disappearance of oxygen atom in the present O_2/CO_2 mixture is caused by reactions 24 and 25.

Reaction 24 is considered to be consisted of the following competing processes.

$$O(^1D) + CO_2 \rightarrow CO_3^* \quad (26)$$

$$CO_3^* \rightarrow CO_2 + O(^3P) \quad (27)$$

$$CO_3^* + M \rightarrow CO_3 + M \quad (28)$$

$$O(^1D) + O_2 \rightarrow O(^3P) + O_2 \quad (29)$$

The γ value is, thus, represented by

$$\gamma = \frac{[CO_2]}{\frac{k_{29}}{k_{26}}[O_2] + [CO_2]} \frac{[M]}{\frac{k_{27}}{k_{28}} + [M]} \quad (30)$$

The values of 1.28×10^{-10} and 4.2×10^{-11} cm^3 molecule^{-1} s^{-1} are employed for k_{26} and k_{29} from the quenching rate constant data in gas phase.[50] The predicted curve from eq 30 is shown in Figure 10b, when the value of k_{27}/k_{28} is selected to be 3×10^{21} molecule cm^{-3}. Provided that the quenching rate constant, k_{28}, is around the same as the values of k_{26} and k_{29}, the value of k_{27} should be equal to $10^{10}-10^{11}$ s^{-1}, which is in a plausible range as a unimolecular decomposition rate constant.

Although eq 30 qualitatively expresses the behavior of γ value as a function of the total density, the quantitative agreement between the prediction and the experimental result is not good, particularly, in the density region larger than 5 mol dm^{-3} as shown in Figure 10b. This deviation might be due to following three mechanisms, namely, (1) the decomposition of CO_4 generated through reaction 25a, (2) the decomposition of ground state CO_3 in the subsequent processes, and/or (3) the cage effect of O_3 photolysis in dense CO_2 media. First, the influence of decomposition of CO_4 generated through reaction 25a to yield atomic oxygen on the γ value is evaluated. When the branching fraction of reaction 16 to 17 as a function of the total density is taken to be the same as the previous value in eq 19, it is found that most of CO_4 decomposes into CO_2 and O_2 through eq 17, and the contribution of CO_4 decomposition for the γ value is smaller than 14% in the total density larger than 5 mol dm^{-3}. Second, CO_3 molecule in the ground state needs about 125 kJ/mol to decompose into CO_2 and $O(^3P)$ according to ab initio calculation by Froese.[41] Thus, the contribution of the reaction, $CO_3 \rightarrow CO_2 + O(^3P)$, is also expected to be relatively small in the present experiment at 308 K, once CO_3^* is stabilized into the ground state. Therefore, the decomposition of CO_4 and/or CO_3 is not a principal reason for the deviation. Next, we will consider the third possibility.

Troe and co-workers once investigated I_2 photodissociation in sub- and supercritical CO_2 and C_2H_6.[6] They found that the quantum yield of I_2 photodisocciation gradually decreased in the high solvent density region from 1 through 20 mol dm^{-3}, which was considered to be due to the cage effect. Similarly, the present deviation between the experimental value and the estimation might be partly ascribed to the cage effect for O_3 photodissociation. However, we will only suggest the possible contribution of the cage effect, because the more quantitative analysis of relevant mechanisms is a formidable task due to the shortage of reliable rate constants of corresponding elementary reactions. For further analysis, we need to develop a technique that realizes the direct observation of intermediate species such as CO_4 and CO_3.

Concluding Remarks

The following conclusions are obtained from the KrF excimer laser photoinduced O_3 formation reaction in O_2/CO_2 mixtures.

1. The predominant pathway of O_3 formation in a O_2/CO_2 mixture is the reaction between the excited $O_2(A\ ^3\Sigma_u^+, A'\ ^3\Delta_u, c\ ^1\Sigma_u^-)$ and ground state CO_2 to form CO_4 intermediate species, and then O_3 is produced from the subsequent reactions.

2. The solvent density effects on the O_3 formation are explained by two processes that have inverse dependence on the solvent density. With the increase of the solvent density, the absorption cross section of Herzberg III system of O_2 is enhanced. On the other hand, the collisional quenching of the CO_4 intermediate species generated from the reaction of $O_2(A,A',c) + CO_2$ causes the decrease of O_3 formation with the increase of the solvent density.

3. During the KrF excimer laser irradiation, the O_3 concentration is kept at a relatively low concentration. The regeneration of O_3 after the photolysis of O_3 may be suppressed due to the reaction between $O(^1D)$ and CO_2 to yield CO_3. The cage effect may also suppress the O_3 photolysis to some extent.

4. Any specific CO_2 pressure effect for the O_3 formation and photodecomposition is not observed in the near-critical region (total density $\approx$ 5 mol dm^{-3}).

Acknowledgment. This work is partly supported by Research for the Future Program of the Japan Society for the Promotion of Science (96P00401), which is greatly appreciated.

References and Notes

(1) Koda, S.; Oshima, Y.; Otomo, J.; Ebukuro, T. *Process Technol. Proc., High-Press. Chem. Eng.* **1996**, *12*, 97.
(2) Koda, S.; Ebukuro, T.; Otomo, J.; Tsuruno, T.; Oshima, Y. *J. Photochem. Photobiol A: Chem.* **1998**, *115*, 7.
(3) Oshima, Y.; Okamoto, Y.; Koda. S. *J. Phys. Chem.* **1995**, *99*, 11830.
(4) Combes, J. R.; Johnston, K. P.; O'Shea, K. E.; Fox, M. A. *ACS Symp. Ser.* **1992**, *488*, 31.
(5) Lienau, C.; Zewail, A. H. *J. Phys. Chem.* **1996**, *100*, 18629.
(6) Otto, B.; Schroeder, J.; Troe, J. *J. Chem. Phys.* **1984**, *81*, 202.
(7) Hippler, H.; Rahn, R.; Troe, J. *J. Chem. Phys.* **1990**, *93*, 6560.
(8) Maneke, G.; Schroeder, J.; Troe, J.; Voβ, F. *Ber. Bunsen-Ges. Phys. Chem.* **1985**, *89*, 896.
(9) Hara, K.; Kiyotani, H.; Kajimoto, O. *J. Chem. Phys.* **1995**, *103*, 5548.
(10) Roberts, C. B.; Zhang, J.; Chateauneuf, J. E.; Brennecke, J. F. *J. Am. Chem. Soc.* **1995**, *117*, 6553.
(11) Worrall, D. R.; Wilkinson, F. *J. Chem. Soc., Faraday Trans.* **1996**, *92*, 1467.
(12) Urdahl, R. S.; Myers, D. J.; Rector, K. D.; Davis, P. H.; Cherayil, B. J.; Fayer, M. D. *J. Chem. Phys.* **1997**, *107*, 3747.
(13) Myers, D. J.; Chen, S.; Shigeiwa, M.; Cherayil, B. J.; Fayer, M. D. *J. Chem. Phys.* **1998**, *109*, 5971.
(14) Peng, D. Y.; Robinson, D. B. *AIChE J.* **1977**, *23*, 137.
(15) Reid, R. C.; Prausnitz, J. M.; Poling, B. E. *The Properties of Gases and Liquid*, 4th ed.; McGraw-Hill: New York, 1987; p 83.
(16) Liu, Z.-Y. *AIChE J.* **1998**, *44*, 1709.
(17) Molina, L. T.; Molina, M. J. *J. Geophys. Res.* **1986**, *91*, 14501.
(18) Press, W. H.; Teukolsky, S. A.; Vetterling, W. T.; Flannery, B. P. *Numerical Recipes in C*; Cambridge University Press: London, 1988; Chapter 14.
(19) Shardanand; Prasada Rao, A. D. *J. Quant. Spectrosc. Radiat. Transfer* **1977**, *17*, 433.
(20) Shardanand, *J. Quant. Spectrosc. Radiat. Transfer* **1977**, *18*, 525.
(21) Amoruso, A.; Crescentini, L. *J. Quant. Spectrosc. Radiat. Transfer* **1995**, *53*, 457.
(22) Johnston, H. S.; Paige, M.; Yao, F. *J. Geophys Res.* **1984**, *89*, 11661.
(23) Blake, A. J.; McCoy, D. G. *J. Quant. Spectrosc. Radiat. Transfer* **1987**, *38*, 113.

(24) Pernot, C.; Durup, J.; Ozenne, J. B.; Beswick, J. A.; Cosby, P. C.; Moseley, J. T. *J. Chem. Phys.* **1979**, *71*, 2387.
(25) Slanger, T. G.; Jusinski, L. E.; Black, G.; Gadd, G. E. *Science* **1988**, *241*, 945.
(26) Shi, J.; Barker, J. R. *J. Geophys Res.* **1992**, *97*, 13039.
(27) Brown, L.; Vaida, V. *J. Phys. Chem.* **1996**, *100*, 7849.
(28) Amimoto, S. T.; Force, A. P.; Wiesenfeld, J. R.; Young, R. H. *J. Chem. Phys.* **1980**, *73*, 1244.
(29) Mack, J. A.; Mikulecky, K.; Wodtke, A. M.*J. Chem. Phys.* **1996**, *105*, 4105.
(30) Hickson, K. M.; Sharkey, P.; Smith, I. W. M.; Symonds, A. C.; Tuckett, R. P.; Ward, G. N. *J. Chem. Soc., Faraday Trans.* **1998**, *94*, 533.
(31) Klatt, M.; Smith, I. W. M.; Symonds, A. C.; Tuckett, R. P.; Ward, G. N. *J. Chem. Soc., Faraday Trans.* **1996**, *92*, 193.
(32) Miller, R. L.; Suits, A. G.; Houston, P. L.; Toumi, R.; Mack, J. A.; Wodtke. A. M. *Science* **1994**, *265*, 1831.
(33) Lauvergnat, D.; Clary, D. C. *J. Chem. Phys.* **1998**, *108*, 3566.
(34) Kenner, R. D.; Ogryzlo, E. A. *Int. J. Kinet.* **1980**, *12*, 501.
(35) Kenner, R. D.; Ogryzlo, E. A. *Can. J. Chem.* **1983**, *61*, 921.
(36) Knutsen, K.; Dyer, M. J.; Copeland, R. A. *J. Chem. Phys*. **1994**, *101*, 7415.
(37) Wildt, J.; Bednarek, G.; Fink, E. H. *Chem. Phys*. **1991**, *156*, 497.
(38) Averyanov, A. S.; Khait, Yu. G.; Puzanov, Yu. V. *J. Mol. Struct. (Theochem.)* **1996**, *367*, 87.
(39) Averyanov, A. S.; Khait, Yu. G.; Puzanov, Yu. V. *J. Mol. Struct. (Theochem.)* **1999**, *459*, 95.
(40) Song, J.; Khait, Yu. G.; Hoffmann, M. R.*J. Phys. Chem. A* **1999**, *103*, 521.
(41) Froese, R. D. J.; Goddard, J. D. *J. Phys. Chem.* **1993**, *97*, 7484.
(42) Ferreira, E.; Gardiol, P.; Sosa, R. M.; Ventura, O. N. *J. Mol. Struct. (Theochem.)* **1995**, *335*, 63.
(43) Castro, M. A. Canuto, S. *Chem. Phys. Lett.* **1991**, *177*, 98.
(44) Benson, S. W. *Thermochemical kinetics*; Wiley & Sons: New York, 1968; Chapter 3. Steinfeld, J. I.; Francisco, J. S.; Hase, W. L. *Chemical kinetics and dynamics*; Prentice Hall: New Jersey, 1989; Chapter 11.
(45) Sedlacek, A. J.; Harding, D. R.; Weston, Jr. R. E.; Kreutz, T. G.; Flynn, G. W. *J. Chem. Phys.* **1989**, *91*, 7550.
(46) Moll, N. G.; Clutter, D. R.; Thompson, W. E. *J. Chem. Phys.* **1966**, *45*, 4469.
(47) Weissberger, E.; Breckenridge, W. H.; Taube, H. *J. Chem. Phys.* **1967**, *47*, 1764.
(48) Jacox, M. E.; Milligan, D. E. *J. Chem. Phys.* **1971**, *54*, 919.
(49) DeMore, W. B.; Jacobsen, C. W. *J. Phys. Chem.* **1969**, *73*, 2935.
(50) Amimoto, S. T.; Force, A. P.; Gulotty, R. G.; Wisenfeld, J. R. *J. Chem. Phys*. **1979**, *71*, 3640.